

Microlens Surveys are a Powerful Probe of Asteroids

Andrew Gould & Jennifer C. Yee

Department of Astronomy, Ohio State University, 140 W. 18th Ave., Columbus, OH 43210, USA; gould,jyee@astronomy.ohio-state.edu

ABSTRACT

While of order a million asteroids have been discovered, the number in rigorously controlled samples that have precise orbits and rotation periods, as well as well-measured colors, is relatively small. In particular, less than a dozen main-belt asteroids with estimated diameters $D < 3$ km, have excellent rotation periods. We show how existing and soon-to-be-acquired microlensing data can yield a large asteroid sample with precise orbits and rotation periods, which will include roughly 6% of all asteroids with maximum brightness $I < 18.1$ and lying within 10° of the ecliptic. This sample will be dominated by small and very small asteroids, down to $D \sim 1$ km. We also show how asteroid astrometry could turn current narrow-angle OGLE proper motions of bulge stars into wide-angle proper motions. This would enable one to measure the proper-motion gradient across the Galactic bar.

Subject headings: gravitational lensing: micro — minor planets, asteroids

1. Introduction

Modern surveys are discovering asteroids in prodigious numbers, soon to exceed a million¹. The applications of such discoveries range from study of the detailed structure of Solar System resonances to defense from (or at least evacuation in the face of) asteroid collisions with Earth. However, despite the exponential increase in asteroid detection, the number of asteroids with well-measured rotation periods and colors (as well as orbital elements) remains quite small. Warner et al. (2009) have assembled a catalog of minor planets with at least some rotation-period information, which in its most recent (November 2012) edition has 5877 entries.² Among these are 1113 main-belt asteroids with excellent period determinations (quality flag ‘3’; excluding ‘3-’).

¹<http://www.minorplanetcenter.net/iau/MPCORB.html>

²<http://www.minorplanet.info/lightcurvedatabase.html>

Figure 1 shows three different views of this sample. The lower and middle panels show differential and cumulative counts as a function of estimated I -band magnitude at opposition. For this purpose, we assumed that inner, middle, and outer main-belt asteroids are at distances of 2.3, 2.9, and 3.4 AU from the Sun. We also assumed $(V - I) = 0.7$ (similar to the Sun). That is, $I = H + 5 \log(x(x - 1)) - 0.7$, where H is the the cataloged absolute magnitude and x AU is the assumed heliocentric distance. There is a clear break at about $I = 11$, a rounding commencing at about $I = 13$, and a sharp drop-off for $I > 16$. The upper panel shows that this drop-off corresponds to asteroid diameters of $D \sim 3$ km in the inner main belt and about $D \sim 20$ km in the outer main belt. Hence, while orbital elements are being measured for vast numbers of asteroids, the rotation periods of small main-belt asteroids are not being probed by current studies.

Observations of Near Earth Asteroids show that objects down to diameters of $D \sim 200$ m have a minimum rotation period of 2.2 hrs (Pravec et al. 2007), presumably because a faster spin exceeds the gravitational binding force. At present there are insufficient numbers of main belt asteroids with measured rotation periods and $D < 3$ km to determine whether they also obey this spin barrier. Dermawan (2004) attempted to address this question by measuring the rotation periods of small main-belt asteroids. However Warner et al. (2009) concluded that none of the rotation periods are secure, i.e., have a quality factor ‘3’.

The fundamental reason that only a tiny fraction ($\sim 10^{-5}$) of the small asteroids being discovered have good rotation periods is that the discovery photometry is very sparse and followup photometry is rare. By contrast, modern bulge microlensing surveys have quite dense sampling, often 10–25 epochs per night. Moreover, these high-cadence zones cover contiguous areas that span 4° or more, meaning that typical asteroids that intersect these fields spend several weeks within them.

One fairly simple idea then, would be just to identify known asteroids passing through these fields and measure their rotation periods (and colors) using archival microlensing data. However, microlensing surveys can have considerably greater return than this for asteroid science. We show here that these surveys can, by themselves, completely characterize the orbits of a large, well-defined subset of asteroids $I < 18.1$ that pass through their high-cadence fields. This means that it is possible to assemble a sample of asteroids that have not only well-defined orbits, rotation periods and colors, but also well-defined selection. By contrast, the present sample of small-to-moderate size asteroids with both rotation periods and orbits is completely heterogeneous.

Thus, present and future microlensing surveys could probe completely new regions of asteroid parameter space.

2. Asteroids in Microlensing Surveys

Our focus here is the possibility of extracting a large statistically well-defined sample of asteroids from existing and planned microlensing data. By “statistically well-defined”, we mean primarily a sample whose orbital elements and selection procedure are well enough understood that the sample can be rigorously compared with a population model that specifies the distributions of orbital elements and (solar system) absolute magnitudes. The (microlensing) data are taken completely without reference to the possibility that asteroids will be or have been detected. Therefore, the key question is: how well can the orbital parameters be measured from existing data? Hence, we will focus mainly on the question of whether orbital elements can be accurately measured from microlensing data alone for a substantial number of asteroids.

2.1. Framing the problem

Microlensing surveys target the Galactic bulge, with the center of high-cadence observations being near (RA,Dec) = (17:58:00,−29:20:00), i.e., 6° south of the Winter Solstice. The size of the high-cadence region varies according to survey. In this study we will adopt the parameters of the OGLE-IV survey and will comment in Section 6 on how the results should be adjusted for other surveys. OGLE-IV surveys an area of 11 contiguous square degrees at least once per hour, with 3/8 of this area being observed three times per hour. Typical trajectories crossing this zone would intersect it for about 4°. This high-cadence region is embedded in a larger low-cadence area³, with one or more observations per night (May–August) over a contiguous area of about 50 deg². These observations are carried out whenever the bulge is visible, except three nights per month, typically chosen to be those when the Moon is passing through the bulge. Seeing of 1” or somewhat higher is achieved on more than half of all nights.

Figure 2 shows the geometry of highly idealized asteroids in co-planar circular orbits. The angles bulge-Sun-Earth and bulge-Sun-asteroid are labeled θ_{\oplus} and θ_{ast} , respectively. By the law of sines

$$\sin \theta_{\oplus} = x \sin \theta_{\text{ast}} \tag{1}$$

where $x\text{AU}$ is the radius of the asteroid orbit. The transverse velocity of the asteroid relative to the Earth is then

$$v_{\text{rel}} = (v_{\text{ast}} - v_{\oplus})_{\perp} = v_{\text{ast}} \cos \theta_{\text{ast}} - v_{\oplus} \cos \theta_{\oplus}. \tag{2}$$

³<http://ogle.astrouw.edu.pl/sky/ogle4-BLG/>

Setting v_{rel} to zero in this equation and combining it with Equation (1) and Kepler’s Third Law yields the orbital phases at which the asteroids are stationary (the transitions from prograde-to-retrograde and retrograde-to-prograde motion)

$$\sin \theta_{\oplus,\text{stat}} = x \sin \theta_{\text{ast},\text{stat}} = \pm \sqrt{\frac{x^2}{1+x+x^2}}. \quad (3)$$

Note that for $x = (2, 3, 4)$, we have $\theta_{\oplus,\text{stat}} = \pm(49^\circ, 56^\circ, 61^\circ)$. Thus, to a good approximation, this defines a zone of retrograde motion during ± 60 days of the Summer Solstice (21 June). We now argue that to a good approximation, asteroids will be discovered if and only if they pass through the high-cadence fields during this “retrograde season”.

There are a number of factors that vary over the course of the “retrograde season”. We will begin by discussing observability and its affects on photometric and astrometric measurements. In Sections 3 and 4 we will examine the impact of additional effects, such as asteroid phase angle and degree of trailing. First note that at the Summer Solstice (and for 15 days on either side) the bulge fields can be observed at airmass < 2 for 10 hours, centered on their transit of the zenith. At 60 days from Summer Solstice, they can be observed for about 4.5 hours on one side of transit and 2 hours on the other. Observations near Summer Solstice therefore have a modest advantage of a longer observing window, which we will see in Section 3.2 scales as $t_{\text{obs}}^{3/2}$, i.e., a factor $(10/6.5)^{3/2} = 1.9$. However, near their turning point the asteroids are moving more slowly and therefore spend more time in the microlensing fields. This effect scales as $v_{\text{rel}}^{-3/2}$. Of course, real asteroids are not on circular co-planar orbits. They could not be observed 6° from the ecliptic if they were. But the point is these two factors go in opposite directions.

On the other hand, most of the asteroids that “enter” the high-cadence fields just after the “retrograde season” has ended are in fact re-entering and were already discovered during the retrograde season. Similarly, those that exit just before the start of the retrograde season, will enter the high-cadence fields at a later point, during the retrograde season. So there are few additional discoveries during these periods. And further from the edges of the retrograde season, the bulge observation window is rapidly contracting, making orbit characterization difficult. Of course, some very interesting asteroids will be discovered during this period, including asteroids interior to the Earth’s orbit and other difficult-to-detect asteroids. However, from the point of view of characterizing the main features of the survey, these are a distraction.

Hence, since the great majority of discoveries will take place during ± 60 days of opposition (Summer Solstice), and since survey geometry does not vary much over this period, we will initially carry out our calculations at Summer Solstice, when the asteroids are at opposition.

Finally we note that while Earth is traveling from $-\theta_{\text{ast,stat}}$ to $+\theta_{\text{ast,stat}}$, the bulge-field observations cover an arc $2\theta_{\text{ast,stat}}$ of an asteroid orbit. At the same time, the asteroids move (in the same direction) through an arc $2\theta_{\oplus,\text{stat}}x^{-3/2}$. Therefore, one season of observations covers a fraction of all asteroids in these orbits of

$$f_{\text{season}} = \frac{\theta_{\text{ast,stat}} - \theta_{\oplus,\text{stat}}x^{-3/2}}{\pi}. \quad (4)$$

For $x = (2, 3, 4)$, we have $f_{\text{season}} = (0.027, 0.029, 0.028)$, i.e., roughly constant. Since, the “cross section” of the high-cadence fields is about 4° , this means that a 10-year survey of this type would detect roughly $(0.028 \text{ yr}^{-1})(10 \text{ yr})(4^\circ/20^\circ) \sim 6\%$ of all asteroids passing within $\pm 10^\circ$ of the ecliptic that satisfy the magnitude limit (still to be established).

Virtually all asteroids discovered in this fashion would have $(V - I)$ colors from OGLE data, and lightcurves spanning of order 40 days (i.e., not just in the high-cadence regions). Since asteroid rotation periods are typically less than one day, these observations would be sufficient to measure the periods, as well as amplitudes of variation, with good precision. Hence they can also be used to identify binaries and measure asteroid shapes.

2.2. Asteroid Detection

Microlensing surveys use difference imaging (Alard & Lupton 1998; Woźniak 2000), in which a reference image is convolved to the seeing of each target image, and then subtracted from it, which removes all non-varying (constant) sources. All that remains are “difference stars” at locations where the flux has changed. These include microlensing events and other stars whose brightness has changed, but it also includes asteroids, whose positions have changed. Microlensing fields are quite crowded, which means that the asteroid will frequently overlap with field stars. However, the great majority of these stars are below the sky background and so will subtract out in the difference image without even adding appreciable noise above the general background. Hence, the signature of an asteroid in these microlensing fields is the same as it would be for a series of images taken of a high-latitude field, i.e., a moving object. The only difference is that bulge fields are more crowded, so occasionally the signal is degraded by confusion with bright or variable stars.

In principle, one could think about finding asteroids that are too faint to detect in individual images by stacking images along (hypothetical) asteroid orbits. However, as we will show below, it is actually impossible to properly characterize the orbits of asteroids that are undetectable in individual images (using microlensing data alone). Since “typical” asteroids are moving at retrograde velocities $v \sim 12 \text{ km s}^{-1}$ at distances $r \sim 2 \text{ AU}$ from Earth, they move only $\sim 30''$ per hour. Hence, in fields with observations at least once per

hour, it is straightforward to identify such tracks on individual nights. Associating tracks between nights is also not difficult. As we will show in Section 5.2, from a single night of data one can predict the position on the next night to within $\mathcal{O}(3'')$, which is extremely precise compared to the surface density of asteroids.

3. Orbit Determination

3.1. Orbit Parameterization

Defining an orbit usually means measuring the six Kepler parameters, i.e., the five invariants of motion plus the orbital phase. However, from the standpoint of understanding the orbital errors, it is more convenient to study the mathematically equivalent parameterization of six Cartesian phase-space coordinates at a given instant of time, i.e., three positions and three velocities. Since the Earth’s orbit is known extremely precisely, these six coordinates are equivalent to the following six: 2 instantaneous angular positions, 2 instantaneous angular velocities, the instantaneous distance, and the instantaneous “radial velocity”, all measured from the center of the Earth. If these six are specified, one can transform to Kepler parameters, and vice versa.

Hence, suppose that one conducts observations over 20 days while an asteroid passes through the high-cadence fields and then considers the ensemble of Kepler models that are consistent with these data. In principle, these models might span a large range of Kepler parameters, but all will agree extremely precisely on the angular positions as seen from the center of the Earth at the instant that the field transits on each night of observations. This is because these quantities are very nearly direct observables. That is, any model that is consistent with the data must reproduce the arc of mean nightly positions of the asteroid, and hence will yield the same angular positions and velocities at a given instant.

These precise nightly determinations have two distinct implications. First they imply that the angular positions and velocities at some fiducial instant near the midpoint of observations are extremely well determined (four parameters). Second, they enable a particularly simple estimate of the measurement precision of the remaining two parameters, i.e., the distance and radial velocity at this same instant. This is because, conceptually, fixing the geocentric angular position and velocity enables one to determine the diurnal parallax offset from each individual astrometric measurement, rather than carrying out a fit to the entire data set. The asteroid-distance measurement on a single night is then a simple integral over these measurements. The standard error of the mean of these measurements then gives the error in the distance at the above fiducial instant, while the error in the slope is the radial-

velocity error. Hence we must begin by deriving the distance error from a single night of data *given* that we know the angular position and velocity at transit.

3.2. Single-night distance measurements

The angular displacement of the asteroid due to diurnal motion of the observatory is $\Delta\boldsymbol{\alpha} = \Delta\mathbf{p}/r$ where $\mathbf{p} = (p_n, p_e)$ is the projected position of the observatory relative to the center of the Earth and r is the asteroid distance. While \mathbf{p} changes in both the north and east directions during the night, the amplitude of the changes in the north component is generally small and will be ignored here in the interest of simplicity. Hence, the precision of the parallax measurement $\pi \equiv \text{AU}/r$ to an asteroid at distance r from Earth derived from n measurements of astrometric precision σ_0 is given by

$$\sigma(\pi) = \pi \frac{\sigma(r)}{r} = \frac{\text{AU}\sigma_0}{\sqrt{n \text{ var}(p_e)}} = 2.2 \times 10^{-3} \left(\frac{n}{10}\right)^{-1/2} \left(\frac{\zeta_e}{0.5}\right)^{-1} \left(\frac{\sigma_0}{30 \text{ mas}}\right) \quad (5)$$

where $\zeta_e \equiv [\text{var}(p_e)]^{1/2}/R_\oplus$ is the standard deviation of observatory motion relative to the Earth center in the east direction normalized to R_\oplus . Hence, for example, the distance of an asteroid at $r = 2 \text{ AU}$ would be measured to a precision of $8.8 \times 10^{-3} \text{ AU}$, assuming the above fiducial parameters. Note that for observations spanning t_{obs} and centered on transit

$$\zeta_e \sim \sqrt{\frac{1 - \text{sinc}(2\pi t_{\text{obs}}/\text{day})}{2}} \cos \delta \rightarrow 0.55 \quad (6)$$

where δ is the latitude of the observatory and where we have assumed that the asteroid declination is similar. The final evaluation assumes $t_{\text{obs}} = 10 \text{ hr}$ and $\delta = -30^\circ$.

Note that in the regime of interest, $1 - \text{sinc}(y) \sim y^2/6 \propto t_{\text{obs}}^2$. Since $n \propto t_{\text{obs}}$, this implies $\sigma(\pi) \propto t_{\text{obs}}^{-3/2}$ as claimed above. More detailed calculations show that this relation remains approximately valid for a time series whose center is somewhat offset from transit, such as those at the limits of the retrograde season.

3.3. Radial velocity measurement

A typical asteroid at opposition moves at about 0.2° per day. Hence it remains in a 4° field for about $T_{\text{obs}} = 20 \text{ days}$. Assuming a fraction f_{gd} of the nights have good seeing and low background, and that these $m = f_{\text{gd}} T_{\text{obs}}/\text{day}$ nights are roughly uniformly distributed

over T_{obs} , then the mean radial velocity will be measured with precision

$$\sigma(v_r) = \sqrt{\frac{12}{m}} \frac{\sigma(\pi)r^2}{T_{\text{obs}}\text{AU}} = 0.81 \text{ km s}^{-1} \left(\frac{n}{10}\right)^{-1/2} \left(\frac{\zeta_e}{0.5}\right)^{-1} \left(\frac{\sigma_0}{30 \text{ mas}}\right) \left(\frac{f_{\text{gd}}}{0.5}\right)^{-1/2} \left(\frac{T_{\text{obs}}}{20 \text{ days}}\right)^{-3/2} \left(\frac{r}{2 \text{ AU}}\right)^2. \quad (7)$$

By contrast, the error in the mean distance (over the measured trajectory) will be $\sigma(\bar{r}) = m^{-1/2}\sigma(\pi)r^2/\text{AU}$. Hence, the ratio of these two errors will be

$$\frac{\sigma(v_r)/v_{\oplus}}{\sigma(\bar{r})/\text{AU}} = \sqrt{12} \frac{\text{AU}}{v_{\oplus} T_{\text{obs}}} = 9.9 \left(\frac{T_{\text{obs}}}{20 \text{ days}}\right)^{-1}. \quad (8)$$

Thus, for typical asteroids at $a \sim 3\text{AU}$, $\sigma(v_r)/v_{\text{ast}} \sim 17\sigma(\bar{r})/a$. This implies that the radial-velocity error is by far the dominant error in the problem. Relative to this error, the five other phase-space coordinates are known with essentially infinite precision.

3.4. Impact on orbital period estimate

In the above approximation that all instantaneous Cartesian parameters except v_r are known perfectly, the specific potential energy is also known perfectly, while the fractional uncertainty in the specific kinetic energy is $2v_r\sigma(v_r)/v_{\text{ast}}^2$, where now v_r is taken to mean the asteroid velocity in the direction of the Earth but the frame of the Sun. Hence, the fractional error in the orbital period P is

$$\frac{\sigma(P)}{P} = \frac{3}{2} \frac{\sigma(a)}{a} = \frac{3}{2} \frac{\sigma(|E|)}{|E|} \sim 3 \frac{v_r\sigma(v_r)}{v_{\text{ast}}^2} = 0.028 \frac{\sigma(v_r)}{0.81 \text{ km s}^{-1}} \frac{v_r/v_{\text{ast}}}{0.2} \left(\frac{v_{\text{ast}}}{17 \text{ km s}^{-1}}\right)^{-1}. \quad (9)$$

Thus, for the above fiducial parameters and a $P = 5$ year orbit, $\sigma(P) \sim 50$ days.

3.5. Astrometric precision and systematic errors

The above estimates were scaled to astrometric measurements of 30 mas. This is a typical error for good-seeing, low-background OGLE-IV stellar images at $I \sim 18.4$ (R. Poleski, private communication 2012). However, asteroid images are not stellar, but trailed. We evaluate the impact of trailing in the Appendix in terms of $\eta \equiv \epsilon/2\sigma$, where ϵ is the length of the trail and σ is the Gaussian width of the point spread function (PSF). This impact is more severe for astrometric measurements in the direction of trailing than the orthogonal direction. Because the astrometry is limited by diurnal parallax measurements, which are essentially East-West and therefore aligned with the direction of asteroid motion (and so trailing), we evaluate the astrometric degradation factor $G_x^{1/2}(\eta)$ in the trailing direction. For

our fiducial geometry, i.e., observations at opposition of an asteroid at $x = 3$ and reasonably good seeing $\sigma = 0.5''$ and 100 s OGLE exposures, we find $\eta = 1$ and therefore $G_x^{1/2}(\eta) = 0.8$. Hence our fiducial precision is achieved at $I = 18.1$.

One must also worry about systematic errors, the most important of which is differential refraction. Asteroids are 1–3 mag bluer in $(V - I)$ than the red giants that mainly define the astrometric reference frame in bulge fields, and the scale of the differential refraction is ~ 7 mas per mag per airmass. Differential refraction is extremely important because the distance measurements in Section 3.2 were based on measuring the astrometric deflection as a function of position relative to the Earth’s center. The latter is very strongly correlated with airmass. Now, differential refraction can be calibrated from stars of similar color to the asteroids. However, (R. Poleski, private communication 2012) finds a systematics error floor of $\sigma_{\text{sys}} \sim 2\text{--}3$ mas, even after correction.

Since these errors are systematic, one cannot necessarily rely on reducing them according to “square-root of N ”, as was assumed in the equations for $\sigma(\bar{r})$ and $\sigma(v_r)$. However, the error floor imposed by systematic errors is very different in the two cases. The measurement of $\sigma(\bar{r})$ will not further improve if $\sigma_0 < \sqrt{nm}\sigma_{\text{sys}}$, whereas for $\sigma(v_r)$ the improvement stops for $\sigma_0 < \sqrt{n}\sigma_{\text{sys}}$. Since the orbit determination is fundamentally limited by the latter, this implies that statistical precision is limited at $\sigma_0 = \sqrt{n}\sigma_{\text{sys}} \sim 10$ mas. Since this is substantially below the fiducial value adopted in Equation (5), the impact of systematic errors is likely to be small.

3.6. Precision of rotation periods and amplitudes

Just as the astrometric precision is degraded by trailing, so is the photometric precision. However, this effect has the same magnitude as the astrometric degradation in the orthogonal direction, $G_y^{1/2}(1) = 0.93$.

At $I = 18.4$ typical OGLE photometry errors are $\sigma(I) \lesssim 0.05$ mag. therefore, we adopt $\sigma(I) \lesssim 0.04$ mag at $I = 18.1$ including the effect of trailing. Small asteroids that would be observed near this limit have (full) amplitudes A of 0.1–0.2 mag. To evaluate the period and amplitude errors, we adopt a simple sinusoidal model: $I(t) = I_0[1 + (A/2) \cos(2\pi t/P_{\text{rot}} + \phi)]$. For N , roughly uniformly sampled data points over time T , the amplitude error is then $[\sigma(A)]^{-2} = (N/T) \int dt (dI/dA)^2$ or

$$\frac{\sigma(A)}{A} = 0.075 \frac{\sigma(I)}{0.04} \left(\frac{A}{0.15}\right)^{-1} \left(\frac{n}{10}\right)^{-1/2} \left(\frac{f_{\text{gd}}}{0.5}\right)^{-1/2} \left(\frac{T_{\text{obs}}}{20 \text{ days}}\right)^{-1/2}, \quad (10)$$

which will therefore typically be quite good.

Similarly, the fractional error (or rather, strictly speaking, the minimum variance bound) in the rotation period is given by $[\sigma(P_{\text{rot}})]^{-2} = (N/T) \int dt (dI/dP_{\text{rot}})^2$ or

$$\frac{\sigma(P_{\text{rot}})}{P_{\text{rot}}} = 0.002 \frac{P_{\text{rot}}}{1 \text{ day}} \frac{\sigma(I)}{0.04} \left(\frac{A}{0.15}\right)^{-1} \left(\frac{n}{10}\right)^{-1/2} \left(\frac{f_{\text{gd}}}{0.5}\right)^{-1/2} \left(\frac{T_{\text{obs}}}{20 \text{ days}}\right)^{-3/2} \quad (11)$$

However, while the amplitude can be estimated directly from the scatter (assuming that the measurement errors are known), the rotation period must be found by testing all possible folds of the lightcurve, via e.g., a periodogram or Fourier transform. This can lead to multiple minima, and hence unless a single period is decisively favored by these tests, the true uncertainty can be much larger than the minimum variance bound. Thus, real data must be fitted before the true period completeness can be assessed as a function of P_{rot} , A , and $\sigma(I)$. See for example Warner & Harris (2011); Harris et al. (2012).

4. Variation of Sensitivity

For simplicity, we have so far evaluated the sensitivity of microlensing surveys under the highly idealized assumption that detections are made at opposition and that asteroids are typically at distance $r = 2 \text{ AU}$ ($x = 3$). We now successively relax these two assumptions.

As the “retrograde season” progresses from opposition toward prograde motion, there are four distinct changes that affect the survey sensitivity: 1) the observation window per night (airmass < 2) shrinks, beginning about 15 days after opposition; 2) the asteroid retrograde motion slows, so that it remains in the high-cadence fields for more nights; 3) the same slowing proper motion decreases the trailing and its consequent error degradation; 4) the asteroid phase angle increases, thus making it fainter. In addition, the distance to the asteroid changes, but this effect is relatively minor. These effects each impact the astrometric and photometric precision differently. Therefore, we examine these two impacts separately.

As discussed in Section 2, the astrometric precision of combined parallax measurements scales as $(v_{\text{rel}}/t_{\text{obs}})^{3/2}$. Since both factors decline during the approach to prograde motion, they tend to cancel. However, in the approximation of co-planer orbits, the first term actually goes to zero, which is both unphysical for extended observations and not actually true for non-co-planar orbits. To suppress this singularity we adopt orbital inclinations of 10° , which is typical for bulge ecliptic latitudes. We then find that the ratio $(v_{\text{rel}}/t_{\text{obs}})$ monotonically declines (improving parallax precision) from opposition to the prograde boundary. For example, it falls by a factor ~ 1.6 at 40 days from the Solstice, implying a factor 2 improvement in astrometric precision. There is also an improvement from decreased trailing, but this improvement is modest because the degradation at opposition is itself minor.

However, these improvements are countered by declining brightness at non-zero phase angle α . To calculate this, we assume a flux factor

$$Z = (1 - g) \exp[-A_1(\tan(\alpha/2))^{B_1}] + g \exp[-A_2(\tan(\alpha/2))^{B_2}] \quad (12)$$

where $A_1 = 3.33$, $A_2 = 1.87$, $B_1 = 0.63$, $B_2 = 1.22$, $g = 0.15$ (Dymock 2007). We then find that the net impact of all three factors on astrometric precision is complex. There is overall degradation from 0 to 35 days after opposition, which peaks at 25% about halfway through. Then there is increasing improvement toward the boundary of the retrograde season.

The photometric precision scales inversely as the square root of the exposure time, $\sim (v_{\text{rel}}/t_{\text{orb}})^{1/2}$, i.e., as the cube-root of the astrometric impact. Curiously, as we show in the Appendix, the impact of trailing on photometric precision also scales as the cube root of its impact on astrometric precision in the range of interest. However, the non-zero phase impacts astrometry and photometry equally. Thus, the overall adverse impact is worse, rising toward 0.45 mag at 35 days and then declining toward zero at the season boundary.

These results imply that the magnitude limit for defining orbits (from microlensing data alone) will vary as a function of phase, up or down by about 0.3 mag relative the special case of opposition, calculated above. Moreover, the rotation-period and variability errors will on average be somewhat larger than those calculated in Section 3.6.

Finally we consider how changing the asteroid orbit impacts these precisions. We find that for other orbital radii, the variation with time from opposition is qualitatively similar to the case examined above for $x = 3$, so that the main differences are found by comparing the cases at opposition. Here there are two effects, both due to the higher proper motion for closer asteroids. First, the time spent in the high-cadence zone is reduced and second, the image trailing is more severe. Together, these nominally lead to a factor 2 decrease in astrometric precision at $x = 2$ relative to $x = 3$. However, because the asteroid is closer, less astrometric precision is actually required to determine its orbit. The most critical measurement is the radial velocity v_r , whose error scales as r^2 . Hence, the orbit determination substantially improves at $x = 2$.

There is also a photometric effect, but this is much smaller, roughly a 0.25 mag degradation at $x = 2$. However, it is important to keep in mind that asteroids of fixed physical characteristics are 9 times brighter at $x = 2$ than $x = 3$.

In summary, the sensitivity of microlensing survey data to asteroids does vary with orbital phase and orbital radius. However, the variations are relatively modest within the “retrograde season” for main belt asteroids. And the key point remains: this sensitivity, while variable, is rigorously calculable for asteroids with any definite set of properties that one might consider.

5. Asteroid Recovery

5.1. Orbital-period timescales

The error in the orbital period given by Equation (9) would be small enough to characterize the asteroid orbit for many purposes. But it would also mean that the asteroid could easily be recovered if it passed through the bulge fields during microlensing season on a previous or subsequent orbit. That is, at any given instant, there would be an essentially one-dimensional, roughly $0.028 * 360^\circ \sim 10^\circ$ track defining the locus of possible positions for reappearance of the asteroid. While there might be other asteroids near this track, the tentative identification of one such image would fix the orbit with essentially infinite precision, which would immediately lead to secure predictions of its position in other images.

What fraction of asteroids could be recovered in this way? Recall from Section 2.1 that about 2.8% of all previously discovered asteroids that pass through high-cadence bulge fields will be detected each year. Ignoring for the moment that the asteroids have a range of inclinations, this means that an average of 2.8% will be recovered each year. Of course, for asteroids on 5 ± 0.5 year orbits, none will be recovered during the first four years, and 14% during the fifth year. Now, if an asteroid has an integer-year orbital period, then it would return to exactly the same place in the high-cadence microlensing field, regardless of inclination. However, if it is highly inclined and does not have an integer-year period, it will likely miss the high-cadence fields. But here it is important to point out that in contrast to the observations required for high-precision orbit determination, the recovery observations can be quite sparse. The regions of such sparse observations are much larger than the high-cadence regions. Moreover, such sparse observations over roughly 50 deg^2 were carried out from 2001-2009 by OGLE-III. Hence, it is likely that tens of percent of asteroids could be recovered using a combination of OGLE-III and OGLE-IV data.

It is quite possible that the great majority of asteroids whose orbits can be characterized by microlensing-survey data will already be known and can simply be matched to entries in the Minor Planet Center database. For example, Polishook et al. (2012) carried out a blind survey using the Palomar Transit Factory, which covered a similar area to the high-cadence OGLE fields with 10 observations per night, for four nights. Of the 30 asteroids that they discovered with $18 < R < 18.5$ (whose faint limit corresponds to $I \sim 18.1$), all were already known. In the next bin $18.5 < R < 19$, only 2 out of 50 were previously unknown.

5.2. Single-night predictions

For completeness, we estimate how well the reappearance of an asteroid can be predicted given a single night of uniformly-spaced data, with n observations over t_{obs} centered at transit, each with σ_0 precision. For this purpose, we approximate the projected motion of the observatory (relative to the Earth center) as $R_{\oplus} \cos \delta \sin(\omega t) \sim R_{\oplus} \cos \delta [\omega t - (\omega t)^3/6]$, where $\omega \equiv 2\pi \text{ day}^{-1}$. Then, if one naively ignores parallax, one will make an error in the geocentric angular velocity $\Delta\mu \simeq \omega R_{\oplus} \cos \delta / r$. This implies that if the distance r is estimated with precision $\sigma(r)$, then the error in μ will be

$$\sigma(\mu) \simeq \omega R_{\oplus} \cos \delta \frac{\sigma(r)}{r^2}. \quad (13)$$

Then, after some algebra, one finds

$$\frac{\sigma(r)}{r^2} = \sqrt{\frac{100800}{n}} (\omega t_{\text{obs}})^{-2} \frac{\sigma_0}{R_{\oplus} \cos \delta}. \quad (14)$$

Together, these imply that the error in the predicted position will be

$$\sigma(\theta) = \text{day} \times \sigma(\mu) = \sqrt{\frac{100800}{n}} \frac{\text{day}}{\omega t_{\text{obs}}^2} \sigma_0 = 2.8'' \left(\frac{n}{10}\right)^{-1/2} \left(\frac{t_{\text{obs}}}{10 \text{ hr}}\right)^{-2} \frac{\sigma_0}{30 \text{ mas}}, \quad (15)$$

independent of distance r .

6. Other Surveys

We have carried out our estimates using the characteristics of the OGLE-IV survey (supplemented by OGLE-III for asteroid recovery). There are two other current microlensing surveys, MOA and Wise, and one planned survey that is well on its way toward commissioning, KMTNet. Because the MOA survey operates from New Zealand, it faces substantially more difficult observing conditions than the OGLE survey does in Chile. The seeing is typically worse and the number of nights with good transparency during the whole night fewer. Combined, these two effects probably degrade the distance measurements by a factor of a few. Nevertheless, the current incarnation of MOA, with 2.2 deg² field and 1.8m telescope has been in operation since 2007. It covers 22 fields (almost 50 deg²) every 50 minutes, which means that the asteroids remain in the MOA fields almost twice as long as in the OGLE fields. Hence many asteroids could be recovered.

The Wise survey (Shvartzvald & Maoz 2012) is carried out from Israel using a 1.0m telescope and 1 deg² camera. Because it is in the northern hemisphere, its observing window

is too short for effective nightly distance measurements. However, being in the northern hemisphere, Wise could make crucial observations that would complement a bulge asteroid survey carried out by either OGLE or MOA. Wise could observe a broad swath toward the Galactic anti-center at low cadence during the northern winter. To recover asteroids, it would only be necessary to make two 2-min observations on each of two successive nights. Hence a campaign of 3 months could cover about 1000 deg^2 , leading to recovery of a large fraction of asteroids over 5 years.

The KMTNet survey will be carried out by three 1.6m telescopes (in Chile, South Africa, and Australia) each with $2^\circ \times 2^\circ$ cameras. The survey plans to monitor four fields with a 10-minute cycle time. Hence, near the Summer Solstice it will observe each field roughly 120 times per night from the two good-seeing sites (Chile and South Africa). It could therefore plausibly reach $2.5 \log(\sqrt{120/10}) = 1.4$ mag deeper than the $I = 18.1$ limit estimated above. And, at fixed magnitude, KMTNet could measure rotation periods much better, if this proves to be a problem for lower-cadence observations. On the other hand fewer asteroids could be recovered from KMTNet data alone, because it does not plan to survey outside the high-cadence fields and because it lacks a long time baseline.

7. Application to Bulge Science

Precise astrometry of asteroids passing through the bulge would enable wide-angle astrometry of the bulge at faint magnitudes. For example, it would permit determination of the proper-motion gradient across the Galactic bar, an important Galactic parameter whose measurement has never even been attempted.

Sumi et al. (2004) measured the proper motions of 5 million Galactic bulge stars with $11 < I < 18$ over 11 deg^2 using OGLE-II data, and R. Poleski (2013, private communication) is in the process of measuring proper motions over about 50 deg^2 using OGLE-III data. These catalogs enable a wide range of bulge science. However, they are intrinsically narrow-angle, i.e., tied to a local reference frame, and so do not permit wide-angle astrometric measurements.

For example, if the bar is inclined to our line of sight by an angle α and is rotating as a solid body at frequency Ω , then after some algebra one finds that the bar proper motion $\Delta\mu(\ell)$ at Galactic longitude ℓ (relative to $\ell = 0$) is given by

$$\Delta\mu(\ell) = (\Omega + \mu_{\text{SgrA}^*}) \sin \ell (\cot \alpha \cos \ell - \sin \ell) - \Omega_U \sin \ell (\cos \ell + \cot \alpha \sin \ell) \quad (16)$$

where $\mu_{\text{SgrA}^*} = -6.38 \text{ mas yr}^{-1}$ (Reid & Brunthaler 2004) is the observed proper motion of SgrA* in the direction of Galactic rotation and $\Omega_U \equiv U_\odot/R_0 \simeq (10 \text{ km s}^{-1})/(8 \text{ kpc}) =$

0.26 mas yr^{-1} reflects the radial motion of the Sun U_{\odot} toward the Galactic center. Hence, ignoring small terms, the gradient of the proper motion is $d\mu/d\ell = (\Omega + \mu_{\text{SgrA}^*}) \cot \alpha - \Omega_U$. It would be interesting to measure both this parameter combination and any deviations from this predicted simple behavior.

There are several possible paths to transforming narrow-angle into wide-angle catalogs. One would be simply to wait for GAIA. A second would be to tie the OGLE proper motions to Tycho-II (Hog et al. 2000). This would require a special set of short exposures taken over several years because essentially all Tycho-II stars are saturated in standard OGLE data. The precision of this approach would be fundamentally limited by the relatively small number of Tycho-II stars ($\sim 200 \text{ deg}^{-2}$), which would yield a precision of 0.20 mas yr^{-1} per deg^2 patch (or 0.22 mas yr^{-1} if $V < 10$ stars were eliminated due to saturation even in shortened exposures). Third, one could tie local OGLE astrometry to UCAC-4 (Zacharias et al. 2013), which in turn is tied to Tycho-II. It is not completely clear that UCAC reductions are effective in crowded bulge fields. Establishing this would require detailed tests. Moreover, this procedure would face the same fundamental limitations as the underlying Tycho-II catalog.

Asteroids with well-defined orbits provide an alternate path to wide-angle proper motions. For example, any asteroid found in OGLE-IV data and recovered in OGLE-III would have an extremely well measured period, as well as other orbital elements. Its predicted position relative to an ensemble of nearby clump giants from the previous orbit would therefore be known to high accuracy for each observation, based on OGLE-IV observations plus the period determined from matching to one position of OGLE-III data. The displacement of the measured position relative to the same ensemble of clump giants in OGLE-III data would then give the relative angular displacement over the elapsed orbital period.

Scaling from the Polishook et al. (2012) detection rate, and assuming 5 years of OGLE-IV searches, a 30% recovery rate from OGLE-III data, and roughly 25 observations for each within OGLE-III, this would imply roughly 11000 measurements with typical precision of 20 mas, spread out over 50 deg^2 . Since the typical elapsed time is 5 years, this leads to proper motion precision of about 0.26 mas yr^{-1} per deg^2 , which is comparable to a calibration based on Tycho-II.

8. Conclusions

We have shown that existing microlensing surveys, particularly the OGLE survey contain a vast wealth of asteroid data from an almost completely untapped region of parameter

space. These data could be exploited to construct a catalog of asteroids with well-measured orbital parameters, precise rotation periods and amplitudes, and essentially perfectly known completeness down to $I \sim 18.1$. Currently, there are about a dozen such asteroids within a magnitude of this limit, and these do not have well-defined completeness properties. These same data can also be used to find asteroid binaries and find asteroid shapes.

This work was supported by NSF grant AST 1103471. J.C. Yee is supported by a Distinguished University Fellowship from The Ohio State University. We thank Scott Gaudi for insightful discussions. We thank David Polishook, Radek Poleski, and David Bennett for important comments on the manuscript. The referee, Petr Pravec, identified a number of key issues whose investigation greatly improved the analysis.

A. Astrometry of Trailed Images

For a general point spread function (PSF), $F(x, y)$ that is normalized to unity, and assuming photon-limited noise, the astrometric error $\sigma_{\hat{\mathbf{n}}}$ in the $\hat{\mathbf{n}}$ directions is given by (e.g., Gould 1995)

$$\sigma_{\hat{\mathbf{n}}}^{-2} = \sum_{ij} \frac{(N\Delta F_{ij}\Delta x\Delta y)^2}{a^2(NF_{ij} + B)\Delta x\Delta y} \quad (\text{A1})$$

where N is the total number of source photons, $(\Delta x, \Delta y)$ is the pixel size, B is the background photon surface density, F_{ij} is the mean of F in pixel (i, j) , and ΔF_{ij} is the change in this number under the impact of a displacement $a\hat{\mathbf{n}}$. If the pixel scale is small compared to the structure of the PSF, then this can be evaluated using,

$$\sigma_{\hat{\mathbf{n}}}^{-2} = N \int dx \int dy \frac{(\hat{\mathbf{n}} \cdot \nabla F)^2}{F(x, y) + B/N}. \quad (\text{A2})$$

We now consider a Gaussian PSF of width σ , that has been trailed by total length ϵ . Since the pixel size is small, we can without loss of generality assume that the trail is in the x direction:

$$F(x, y) = \frac{\exp(-y^2/2\sigma^2) \int_{-\epsilon/2}^{\epsilon/2} d\ell \exp(-(x + \ell)^2/2\sigma^2)}{2\pi\sigma^2\epsilon} \quad (\text{A3})$$

from which we derive

$$\frac{dF}{dx} = \frac{\exp(-y^2/2\sigma^2)}{2\pi\sigma^4\epsilon} \left[e^{-(x+\epsilon/2)^2/2\sigma^2} - e^{-(x-\epsilon/2)^2/2\sigma^2} \right], \quad (\text{A4})$$

and

$$\frac{dF}{dy} = \frac{-y}{\sigma^2} F(x, y). \quad (\text{A5})$$

We now restrict to the background-limited case, i.e., $F(x, y) + B/N \rightarrow B/N$ in the denominator of Equation (A2). We then obtain for the trail direction,

$$\sigma_{\hat{x}}^{-2} = \frac{N^2}{8\pi\sigma^4 B} G_x(\eta); \quad G_x(\eta) \equiv \frac{1 - \exp(-\eta^2)}{\eta^2}; \quad \eta \equiv \frac{\epsilon}{2\sigma} \quad (\text{A6})$$

We recognize the first factor as the standard expression for the astrometric error of a Gaussian PSF below sky. The second term quantifies the degradation due to trailing. In the limit of $\eta \ll 1$, $G_x(\eta) \rightarrow 1 - \eta^2/2$, implying that the error is fractionally degraded by $\eta^2/4$. For the intermediate case, $\eta = 1$ (e.g., $\epsilon = 1''$ and $\text{FWHM} \simeq 1.2''$) the error degradation is $G_x^{1/2} \rightarrow 0.80$. For long trails, $G_x^{1/2} \rightarrow \eta^{-1}$.

For the non-trailed direction, the astrometric precision is

$$\sigma_{\hat{y}}^{-2} = \frac{N^2}{8\pi\sigma^4 B} G_y(\eta); \quad G_y(\eta) = \frac{\sqrt{2\pi}}{8\eta^2} \int_{-\infty}^{\infty} dz [\text{erf}(z + \eta/\sqrt{2}) - \text{erf}(z - \eta/\sqrt{2})]^2 \quad (\text{A7})$$

This cannot be evaluated in closed form, but in the three regimes evaluated above, $G_y^{1/2}(\eta) = 1 - \eta^2/12$ ($\eta \ll 1$); $G_y^{1/2}(1) = 0.93$; $G_y^{1/2}(\eta) = \pi^{1/4}\eta^{-1/2}$ ($\eta \ll 1$).

Finally, we note that it is straightforward to show that the photometry precision of a trailed image is degraded by exactly the same factor $G_y^{1/2}$ as the non-trail direction astrometry.

(A8)

REFERENCES

- Alard, C. & Lupton, R.H. 1998, *ApJ*, 503, 325
- Dermawan, B., 2004. Spin characteristics of very small main-belt asteroids. Ph.D. thesis, School of Science, The University of Tokyo
- Dymock, R. 2007, *Journal of British Astronomical Association*, 117, 6
- Gould, A. 1995, *ApJ*, 440, 510
- Harris, A.W., Pravec, P. & Warner, B.D., 2012, *Icar*, 221, 226
- Hog, E., Fabricius, C., Makarov, V.V., et al. 2000, *A&A*, 355, L27
- Polishook, D., Ofek, E.O., Waszczak, A. et al. 2012, *MNRAS*, 421, 2094

- Pravec, P., Harris, A. W., & Warner, B. D. 2007, in IAU Symposium, Vol. 236, IAU Symposium, ed. G. B. Valsecchi, D. Vokrouhlický, & A. Milani, 167–176
- Reid, M.J. & Brunthaler, A. 2004, ApJ, 616, 872
- Shvartzvald, Y. & Maoz, D. 2012, MNRAS, 419, 3631
- Sumi, T., Wu, X., Udalski, A., et al. 2004, MNRAS, 348, 1439
- Warner, B.D., Harris, A.W., & Pravec, P. 2009, Icar, 202, 134
- Warner, B.D. & Harris, A.W. 2012, Icar, 216, 610
- Woźniak, P.R. 2000, Acta Astron 50, 421
- Zacharias, N., Finch, C., Girard, T., et al. 2013, AJ, 145, 44

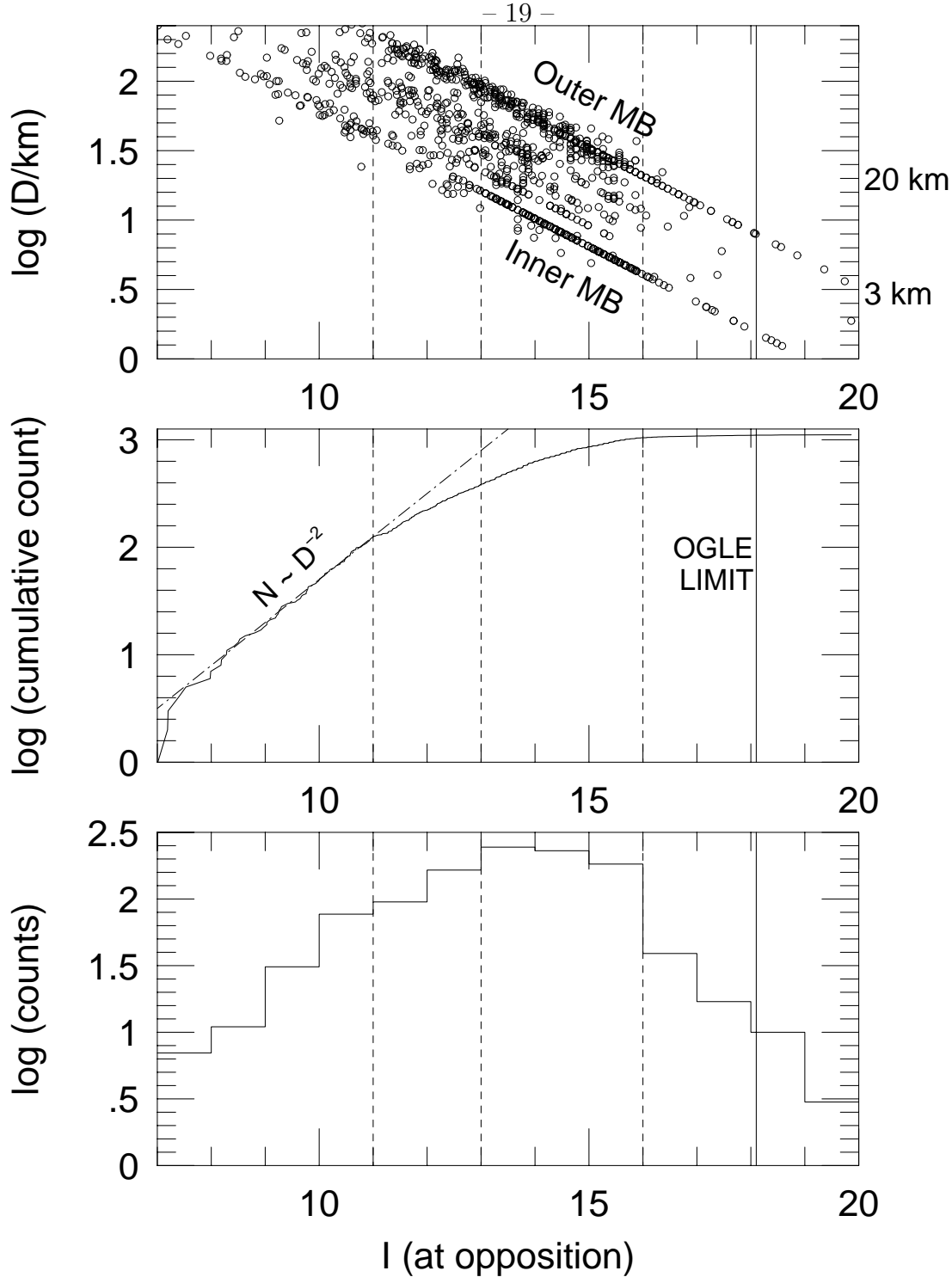


Fig. 1.— Lower and middle panels: Differential and cumulative number counts of asteroids with excellent rotation-period determinations as a function of estimated I -band magnitude at opposition as derived from the Nov 2012 update of Warner et al. (2009). Apparent breaks in the distribution are indicated by dashed vertical lines: below $I = 11$, the distribution obeys a diameter distribution $N \propto D^{-2}$ (dot-dashed line), it begins to turn over at $I = 13$, and suffers a rapid drop-off for $I > 16$. This is compared to our estimated completeness limit from an OGLE-based survey of $I = 18.1$. Upper panel: estimated diameters of these same cataloged asteroids. Very few are smaller than 3 km.

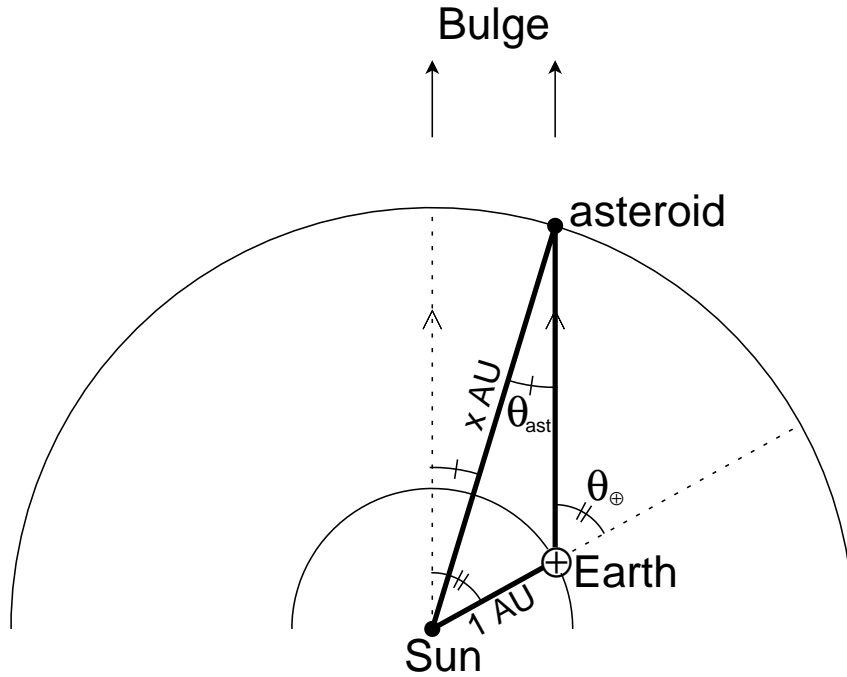


Fig. 2.— Idealized geometry of asteroids passing through bulge microlensing fields. As the Earth moves (orbital phase θ_{\oplus}) in its approximately circular orbit, the observations target the same bulge fields. The angle bulge-Sun-asteroid to an asteroid at x AU can therefore be calculated from the law of sines: $\sin \theta_{\text{ast}} = x^{-1} \sin \theta_{\oplus}$. If the asteroid orbit is approximated as circular, then at $\theta_{\oplus} = \theta_{\oplus, \text{stat}} = \sin^{-1}[x(1+x+x^2)^{-1/2}]$ the asteroids transition from prograde to retrograde motion (or vice versa). See Equation (3). Specifically, $49^\circ < \theta_{\oplus, \text{stat}} < 61^\circ$ for $2 < x < 4$. The season when many new asteroids can be discovered is approximately $2\theta_{\oplus, \text{stat}}$. The fraction of asteroids discovered during this time is $f_{\text{season}} = [\theta_{\text{ast, stat}} - \theta_{\oplus, \text{stat}}x^{-3/2}]/\pi$, i.e., 2.7%–2.9% per season.